JOURNAL OF BACTERIOLOGY, Nov. 2007, p. 7896–7910 Vol. 189, No. 21
0021-9193/07/$08.00+0 doi:10.1128/JB.00726-07

Antigen 84, an Effector of Pleiomorphism in *Mycobacterium smegmatis*▽

Liem Nguyen,[1,2,3] Nicole Scherr,[2] John Gatfield,[2] Anne Walburger,[2] Jean Pieters,[2]* and Charles J. Thompson[2,3]*

Department of Molecular Biology and Microbiology, School of Medicine, Case Western Reserve University, Cleveland, Ohio 44106[1]; Biozentrum, University of Basel, Klingelbergstrasse 50/70, CH-4056 Basel, Switzerland[2]; and Life Sciences Centre, University of British Columbia, 2350 Health Sciences Mall, Vancouver, British Columbia V6T 1Z3, Canada[3]

Received 9 May 2007/Accepted 23 August 2007

While in most rod-shaped bacteria, morphology is based on MreB-like proteins that form an actin-like cytoskeletal scaffold for cell wall biosynthesis, the factors that determine the more flexible rod-like shape in actinobacteria such as *Mycobacterium* species are unknown. Here we show that a *Mycobacterium smegmatis* protein homologous to eubacterial DivIVA-like proteins, including *M. tuberculosis* antigen 84 (Ag84), localized symmetrically to centers of peptidoglycan biosynthesis at the poles and septa. Controlled gene disruption experiments indicated that the gene encoding Ag84, *wag31*, was essential; when overexpressed, cells became longer and wider, with Ag84 asymmetrically distributed at one pole. Many became grossly enlarged, bowling-pin-shaped cells having up to 80-fold-increased volume. In these cells, Ag84 accumulated predominantly at a bulbous pole that was apparently generated by uncontrolled cell wall expansion. In some cells, Ag84 was associated with exceptional sites of cell wall expansion (buds) that evolved into branches. *M. bovis* BCG Ag84 was able to form oligomers in vitro, perhaps reflecting its superstructure in vivo. These data suggested a role for Ag84 in cell division and modulating cell shape in pleiomorphic actinobacteria.

Bacteria have been traditionally recognized by their size, the chemical composition of their cell envelopes, and their distinctive shapes. All of these features are thought to be determined by targeted activities of a family of well-conserved enzyme complexes that synthesize the peptidoglycan polymers making up their rigid cell walls (28). Temporal and spatial control of these enzyme complexes during growth and division are coordinated by proteins of the bacterial cytoskeleton (8). Together, these mechanisms of regulated expansion of the cell wall determine the characteristic size and shape (spherical, rod shaped, or filamentous) of individual bacterial species (17, 69). Some bacteria, such as those belonging to the actinomycete taxon, are unusual in that they have evolved mechanisms to transform themselves into different shapes.

Studies of rod-shaped bacteria such as *Bacillus subtilis* and *Escherichia coli* have identified at least 15 genes needed for assembly of peptidoglycan in the cell wall (24) and generated a model (34) in which extension of their basic tubular structure is periodically interrupted and coordinated with synthesis of the division septum (34, 59). In this model, lateral extension and division are mutually exclusive assembly processes (34) carried out by different peptidoglycan biosynthetic machineries (52). Lateral extension is dependent on a family of at least three penicillin binding proteins (PBPs); septum formation involves at least nine late-division proteins, including PBP2b in *B. subtilis* (52) and its homolog PBP3 in *E. coli* (FtsI) (28).

To maintain a tubular shape during lateral extension, rod-shaped bacteria utilize multiple copies of MreB and MreB-like proteins (Mbl) to construct cytoskeleton-like structures that determine the sites of cell wall synthesis (7, 17, 21, 69). In *B. subtilis*, nascent peptidoglycan accumulates in a helical pattern within the lateral wall, as directed by Mbl (17) and perhaps other partners (7, 63). Systems that control the width and length of the cylinder are dependent on MreB and Mbl, respectively (30). Coordinated remodeling of this cytoskeletal scaffold allows the bacterium to increase in length while retaining a rod shape (9, 32). Undefined indicators of growth eventually trigger an alternative cell wall biosynthetic mechanism for septum formation and cell division.

Septum formation is dependent on the recruitment of the late-division proteins into the site of the division septum, a process that is initiated by the assembly of the FtsZ protein into a ring structure, normally at the midcell of rod-shaped bacteria. There are two mechanisms for positioning the FtsZ ring that operate by restricting its formation either at the midcell or near the poles (documented and reviewed in references 6, 24, 35, 50, and 59). Nucleoid occlusion prevents septum formation along the central part of the rod until it is vacated by the segregating chromosomes (4, 41, 66, 68). Proteins that effectuate nuclear occlusion may be involved in ring-assembly site selection or stabilization (for example, SlmA in *E. coli* [4] and Noc in *B. subtilis* [68]). This mechanism does not exclude initiation of division septa in regions more proximal to the poles. The MinCD system prevents cell division at these sites by inhibiting FtsZ ring formation (29, 54, 55). In *E. coli*, a complex of MinC and MinD proteins oscillates between the two poles (29, 48), thereby providing a concentration minimum at the midcell. In *B. subtilis*, the DivIVA protein retains MinC and MinD at the cell poles, thus targeting the midcell for septum formation (11, 19, 36, 37). Other mechanisms, not associated with a previous division septum, must exist to reas-

* Corresponding author. Mailing address for Charles J. Thompson: Department of Microbiology and Immunology, Life Sciences Centre, University of British Columbia, 2350 Health Sciences Mall, Vancouver, B.C., Canada V6T 1Z3. Phone: 604-822-2501. Fax: 604-822-6041. E-mail: charles.thompson@ubc.ca. Mailing address for Jean Pieters: Department of Biochemistry, Biozentrum, University of Basel, 50-70 Klingelbergstrasse, Basel, Switzerland CH4056. Phone: 41 61 267 2151. Fax: 41 61 267 2148. E-mail: Jean.Pieters@unibas.ch.

▽ Published ahead of print on 31 August 2007.

TABLE 1. Plasmids and primers used in this study

Plasmid or primer	Relevant genotype[a]	Source or reference
Plasmids		
pGEM-T Easy	*bla lacZ* ori_{pUC}	Promega
pEGFP	*bla* P_{lacZ}*-egfp* ori_{pUC}	Clontech
pMV361	*aph* P_{hsp60} *att-int*^{L5} *colE1*	60
pJAM2	*aph* P_{ace} *oriM colE1*	64
pYUB328	*bla colE1 cos*^{l}	2
pYUB854	*res-hyg-res colE1cos*^{l}	3
pNDL1	*aph* P_{hsp60}*-wag31*$_{MS}$*-gfp att-int*^{L5} *colE1*	This study
pNDL2	*aph wag31*$_{MS}$*-gfp colE1* (*pNDL1–att-int*^{L5} deletion)	This study
pNDL4	*aph* P_{hsp60}*-wag31*$_{MS}$ *att-int*^{L5} *colE1*	This study
pNDL5	*aph* P_{ace}*-wag31*$_{MS}$ *oriM colE1*	This study
pNDL6	*res-5′div-hyg-3′div-res colE1cos*^{l}	This study
pNDL8	*aph* P_{hsp60}*-wag31*$_{TB}$ *att-int*^{L5} *colE1*	This study
phAE87	*TM4ts*::*pYUB328*	10
phNTL2111	*TM4ts*::*pNDL6*	This study
Primers		
VN1	*AAGCTTGAATTCCAT*ATGCCGCTCACACCAGCGGAC	Microsynth
VN2	*GACCGGTACCGG*GTTGTTGCCGCGGTTGAACTGGC	Microsynth
VN3	*GGATCCGAATTCCAT*ATGCCGCTCACACCAGCGGAC	Microsynth
VN5	*TCTAGAAAGCTT*TCAGTTGTTGCCGCGGTTGAACTG	Microsynth
VN6	*GGTACCGCGGCCGC*TCGCATCACCGGTCGGCACAC	Microsynth
VN7	*TCTAGA*TGTCTGCCCCCTTGAAGTCTTGAAC	Microsynth
VN8	*AAGCTT*CTGACTCGATGGGTCCGTCACC	Microsynth
VN9	*CTCGAGACTAGT*GCTAGTTCTTGCGCTCTTCGGTCT	Microsynth
VN10	*GAATTCCAT*ATGCCGCTTACACCTGCCGACG	Microsynth
VN11	*GGATCCAAGCTT*CTAGTTTTTGCCCCGGTTGAATTGATC	Microsynth

[a] Restriction sites are shown in italics. $_{MS}$, *M. smegmatis*; $_{TB}$, *M. tuberculosis*.

semble DivIVA at a new site of growth during spore germination (26).

Distinctive mechanisms to generate new poles must have evolved in filamentous bacteria such as *S. coelicolor*, where growth and genome replication typically do not lead to cell division (17, 23). The paradigm established with respect to unicellular rod-shaped bacteria, where cell wall biosynthesis cycles between polar and lateral sites, does not apply to *S. coelicolor* (17), where cell wall growth occurs continuously, primarily at the tip of extending filaments, and may be dependent on DivIVA (22). Branching, needed for maintaining quasiexponential growth, may also be DivIVA dependent (22, 23). In *S. coelicolor*, DivIVA is essential; when overexpressed, it is associated with randomly distributed swollen foci within the lateral cell wall. The foci mature into branches, suggesting that DivIVA may play a direct or indirect role in generating new sites of cell wall biosynthesis in these filamentous organisms (22). DivIVA may recognize unidentified molecular markers or the physical shape of the cell wall (20) to generate branches (22). Continued overexpression leads to enlarged ovoid cells and lysis. These effects indicate that overexpression of DivIVA modifies the standard mechanism for shape determination and cannot be readily explained by osmotic distortions of a weakened cell wall (22). Similarly, overexpression of DivIVA in *Corynebacterium* species results in diverse changes in cell morphology (47).

The fact that many genes that control cell shape and growth (by encoding, e.g., MreB, Mbl, MinC, and MinD) are absent in *Mycobacterium* genomes suggested that DivIVA interacts with other partners to regulate shape in these pleiomorphic organisms. While *Mycobacterium* species are primarily rod-like in shape, careful microscopic examination has revealed that they can have different shapes and sizes. For example, *Mycobacterium tuberculosis* cells can become shorter in older cultures (43), filamentous within macrophages (13), and ovoid during carbon starvation (44) and can generate microscopic "bleb"-like structures on the surface in stationary-phase cultures (16) that may mature into larger buds and branches (15). While molecular mechanisms that affect such changes are not well understood, several proteins have been associated with changes in morphology. Overexpression of the *pknA* serine threonine kinase, resulting in phosphorylation of a specific residue in *M. tuberculosis* antigen 84 (Ag84), generated shorter and broader cells in liquid cultures (31). Moderate induction of Ag84 transcription during the stationary phase had a similar effect on morphology which appeared to be dependent on phosphorylation (31). A genome-wide analysis (using transposon site hybridization) indicated that Ag84 might be essential in *M. tuberculosis* (51). In this paper, we show that Ag84, a DivIVA homologous protein, is essential, localizes at the cell poles, affects polar growth, and may, directly or indirectly, influence cell division and morphological alternatives in *Mycobacterium smegmatis*.

MATERIALS AND METHODS

Bacterial strains and plasmids. The plasmids used are listed in Table 1. *M. smegmatis* wild-type mc^{2}155 (57) and its derived strains were grown at 37°C in 7H9 liquid medium and 7H10 agar (Difco) supplemented with 0.2% glucose, 0.5% glycerol, and 0.5% Tween 80. Kanamycin and hygromycin were used at final concentrations of 50 μg ml^{-1} and 100 μg ml^{-1}, respectively. *Mycobacterium bovis* BCG was grown in the same media supplemented with OADC (oleic acid-albumin-dextrose-catalase; Difco). *E. coli* XL1-Blue (Stratagene) was used for subcloning procedures and was grown in LB medium.

Construction of *wag31* expression strains. Primers VN3 and VN5 were used for PCR amplification of the $wag31_{MS}$ gene from *M. smegmatis* genomic DNA using poly(A) Easy enzyme (Stratagene). PCR product was TA cloned into pGEM-T Easy vector, and its sequence was verified. The DNA fragment was then cloned downstream of the constitutive promoter P_{hsp60} in pMV361 (EcoRI, HindIII-pNDL4) or the acetamide-inducible promoter in pJAM2 (64) (BamHI, XbaI-pNDL5). Primers VN10 and VN11 were used to amplify the $wag31_{TB}$ gene from *M. tuberculosis* genomic DNA and cloned into pMV361 (EcoRI, HindIII-pNDL8). Vectors pNDL4, pNDL5, and pNDL8 were used to transform *M. smegmatis* wild-type mc^2155 to generate strains NDL4, NDL5, and NDL8, respectively.

Construction of $wag31_{MS}$-*gfp* fusions. $wag31_{MS}$ was amplified by PCR (primers VN1 and VN2) and was cloned into pEGFP by use of HindIII and KpnI sites. This created a translational fusion, $wag31_{MS\text{-}gfp}$, in which a linker (PVPVAT) separated the C terminus of *M. smegmatis* Ag84 ($Ag84_{MS}$) from the N terminus of green fluorescent protein (GFP). The fusion gene was removed from pEGFP by digestion with EcoRI. Plasmid pNDL1 was constructed by cloning the $wag31_{MS\text{-}gfp}$ fusion fragment into the EcoRI site of pMV361 (60). Its orientation was checked by restriction digestion and sequencing. The NdeI DNA fragment containing the heat shock promoter and the integrase gene in pNDL1 was removed, and the remaining fragment was religated to create pNDL2. A control fusion was created by cloning the *gfp* gene translationally fused to the heat shock promoter P_{hsp60} and the ribosome binding site in pMV361.

Disruption of the chromosomal $wag31_{MS}$. $wag31_{MS}$ deletion in *M. smegmatis* was done essentially as described previously (3). Primers VN6 and VN7 were used to amplify the 5′ upstream flanking arm of $wag31_{MS}$ (*5′div*). VN8 and VN9 were used to amplify the 3′ downstream flanking arm of $wag31_{MS}$ (*3′div*). These fragments were inserted into pYUB854 on either side of the hygromycin resistance gene to generate pNDL6. This recombinant cosmid was cloned into the unique PacI site of phAE87, replacing the built-in cosmid pYUB328, and were in vitro packaged using GIGAPack III GOLD packaging extracts (Stratagene). Transduced *E. coli* NM554 was plated on hygromycin-containing LB agar plates. Phasmid DNA (phNTL2111) prepared from a pool of hygromycin-resistant transductants was electroporated into *M. smegmatis* mc^2155. Phage plaques that grew at permissive temperature (28°C) were purified, checked for temperature sensitivity, and then used to transduce *M. smegmatis* cells. Hygromycin-resistant colonies were selected on 7H10-ADC medium at nonpermissive temperature (37°C).

Preparation of *M. bovis* BCG lysates. For gel filtration and cross-linking experiments *M. bovis* BCG cultures were harvested at an optical density at 600 nm of 0.7 to 0.9. Cells were washed three times in phosphate-buffered saline (PBS) and disrupted in the presence of glass beads and protease inhibitors (phenylmethylsulfonyl fluoride and complete EDTA-free protease inhibitor cocktail from Roche) by using a mixer mill (type MM 300; Retsch, Germany) at a frequency of 30 cps for 20 min with chilling intervals. Cell debris and nonlysed cells were removed by low-speed centrifugation (10 min at 10,000 rpm).

For cell fractionation, bacteria were washed twice in PBS followed by a final washing step and were resuspended in TEN buffer (75 mM Tris [pH 8.8], 4 mM EDTA, 100 mM NaCl). Cells were lysed in the presence of protease inhibitors by three passages through a French press (Thermo, Waltham, MA). Cell lysate was cleared by centrifugation (10 min at 10,000 rpm).

SDS-PAGE. Sodium dodecyl sulfate-polyacrylamide gel electrophoresis (SDS-PAGE) (33) was performed using a Bio-Rad Protean II system. Equal amounts of protein (5 to 15 μg) were loaded per lane. The samples were heated for 7 min at 95°C, centrifuged briefly, and loaded onto 10% or 12.5% SDS-PAGE gels.

Immunoblotting. Samples were treated with SDS loading buffer and boiled for 7 min, and 10 μg lysate was loaded per lane on a 12.5% SDS-PAGE gel. Western blot analysis was performed according to standard protocols (5) using a mouse monoclonal antibody against mycobacterial Ag84 (F126-2; a kind gift from A. Kolk, KIT Biomedical Research, Amsterdam, The Netherlands). The secondary antibody, anti-mouse immunoglobulin G coupled to horseradish peroxidase (Amersham), was visualized by chemiluminescence.

Affinity purification of Ag84. Monoclonal antibody F126-2 (7 mg ml^{-1} protein concentration) in buffer containing 0.2 M $NaHCO_3$ and 0.5 M NaCl (pH 8) was coupled to an *N*-hydroxysuccinimide-activated column (Pharmacia), following instructions of the manufacturer. The column was washed with buffer A (100 mM glycine; pH 2.5) and equilibrated in buffer B (50 mM Tris-HCl [pH 8], 150 mM NaCl) at 0.15 ml min^{-1}. An *M. bovis* BCG cell pellet was resuspended in buffer B containing 1 mM phenylmethylsulfonyl fluoride and protease inhibitor cocktail. The cell slurry was disrupted by use of a French press and centrifuged at 18,000 rpm and 4°C for 60 min, filtered through 0.45 μm filters, and loaded onto the column at 0.15 ml min^{-1}. Unbound proteins were washed at 1 ml min^{-1} until the optical density at 280 nm reached the baseline value. Proteins were eluted with buffer A into 0.5 ml fractions and immediately neutralized with 25 μl of 2 M Tris-HCl, pH 8. Fractions containing Ag84 were detected on Western blots by use of F126-2 antibody.

Cell fractionation. Total lysate was subjected to a high-speed spin (100,000 × *g*) to obtain a membrane and soluble fraction. Western blot analysis was performed as described above. Monoclonal antibodies GroEL AI-75320 (MRL; Department of Microbiology, Fort Collins, CO) and lipoprotein F29-47 (kind gift from A. Kolk, KIT Biomedical Research, Amsterdam, The Netherlands) were used as controls.

Chemical cross-linking. Purified Ag84 (0.2 mg ml^{-1}) or *M. bovis* BCG lysate (1 mg ml^{-1}) was added with the indicated concentrations of formaldehyde and incubated for 15 min at 37°C. Samples were treated with SDS buffer and loaded on a 10% SDS-PAGE gel followed by Western blotting with Ag84 antibody.

Size-exclusion chromatography. *M. bovis* BCG lysate (in a soluble fraction prepared as described above) (50 μg) was applied to a gel filtration column (Superdex 200 PC 3.2/30; Pharmacia) preequilibrated in PBS. The presence of Ag84 in the collected fractions was detected by immunoblotting. Standard marker proteins (Bio-Rad) were bovine thyroglobulin (670 kDa), bovine γ-globulin (158 kDa), chicken ovalbumin (44 kDa), horse myoglobin (17 kDa), and vitamin B_{12} (1.35 kDa).

Microscopy. Nascent peptidoglycan synthesis labeling was done as described previously (17). Briefly, 2 μg ml^{-1} BODIPY FL-conjugated vancomycin (Invitrogen) was added to growing cultures. The cultures were then incubated for 2 to 3 h to allow binding of the labeled antibiotic within the cell wall. Cells were viewed directly or after fixation with 2% formaldehyde for 30 min at room temperature. Fixed cells were mounted on poly-L-lysine-coated slides (PolyScience) and washed three times with PBS. Membranes were visualized by incubating slides for 5 min in 1.5 μg ml^{-1} FM4-64.

Samples were mounted using FluoroGuard antifade mounting medium (Bio-Rad). Specimen observation and image acquisition were performed using a confocal laser-scanning module LSM510 Meta (Zeiss) connected to an Axiovert 200 M microscope (Zeiss). The pinhole was adjusted to obtain confocal layer heights between 0.6 and 0.9 μm.

For time-lapse movies, growing cultures were placed on a pad of 1.5% agarose made in 7H9 medium. Three-hour sequences (10 min intervals) were recorded by video microscopy using a digital camera (Hamamatsu Photonics, Japan) connected to a Zeiss Axiophot microscope equipped with a temperature (37°C)-controlled and CO_2 (5%)-equilibrated chamber and Openlab software (version 2.0).

To measure size, bacterial cells from colonies grown on 7H10 agar supplemented with OADC and 25 μg ml^{-1} kanamycin were resuspended in 7H9 liquid medium and diluted to a density of 10 to 20 cells per microscopic focal plane. At various times after transformation, around 100 bacterial cells were measured (length, the maximum distance between the two cell poles; width, largest diameter of examined cell).

To analyze the localization of Ag84, *M. smegmatis* overexpressing $wag31_{MS\text{-}gfp}$ was grown on 7H10 agar supplemented with OADC and 25 μg ml^{-1} kanamycin. Cells were resuspended in 7H9 medium, and around 100 cells were analyzed each day during cultivation. Ag84 localization was considered asymmetric when the cell poles contained different amounts of Ag84 and was regarded as symmetric when Ag84 was equally distributed at both poles.

Low-temperature scanning electron microscopy was carried out as described previously (42). Thin-section samples for transmission electron microscopy (TEM) studies were prepared as described previously (45), and pictures were taken using a Philips 401 electron microscope. Immunocytochemistry analysis was performed using F126-2 antibody and a Philips CM10 electron microscope (65).

RESULTS

***wag31* encodes the mycobacterial DivIVA homolog known as antigen 84.** To search for genes potentially involved in mycobacterial growth or cell division, updated databases were screened for orthologs of MreB or DivIVA. While MreB-like proteins are thought to determine lateral growth in more than 400 different bacteria classified into many bacterial subdivisions (classified as "Cell shape determining protein" MreB/Mbl in the InterPro database [http://www.ebi.ac.uk/interpro/IEntry?ac=IPR004753]), they are rarely found in actinobacteria (Fig. 1A) (38). On the other hand, DivIVA-like proteins were

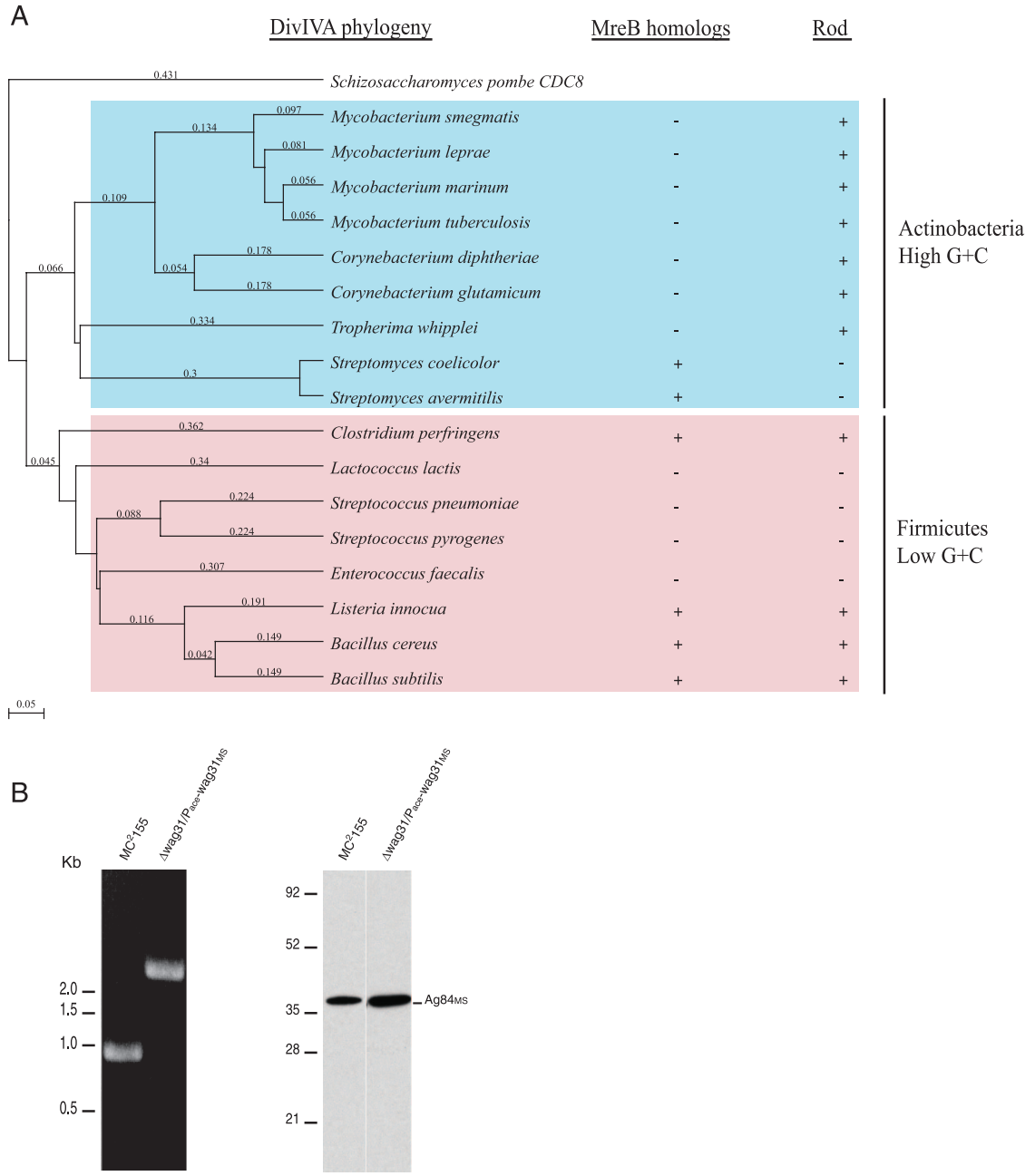

FIG. 1. The DivIVA homolog in mycobacteria. (A) Phylogenetic representation of DivIVA-like proteins from gram-positive bacteria in relation to morphology and the presence of MreB-like proteins. In firmicutes, the presence of MreB correlates with a rod shape, while in most rod-like, sometimes pleiomorphic, actinobacteria, MreB is not present. Protein sequences were obtained from the National Center for Biotechnology Information (http://www.ncbi.nlm.nih.gov/genomes/lproks.cgi) and the TIGR genome databases (www.tigr.org/). Alignment of protein sequences was carried out using the ClustalW algorithm (62). The tree was generated using the UPGMA algorithm in the MacVector 8.0 package (Accelrys Inc., San Diego, CA). A distance bar is shown under the tree. (B) The *M. smegmatis* gene encoding $Ag84_{MS}$ (*wag31*$_{MS}$) is essential. The chromosomal *wag31*$_{MS}$ could only be disrupted by phage-mediated allelic exchange when wild-type *M. smegmatis* was supplemented in *trans* with a vector expressing *wag31*$_{MS}$ from the acetamidase promoter. The disruption was confirmed by recovering the mutant locus by PCR using primers flanking the putative open reading frame. The mutant gene containing the inserted hygromycin resistance cassette generated a larger fragment (left panel). $Ag84_{MS}$ expression of the chromosomal *wag31*$_{MS}$-deleted mutant was detected by Western blotting using antibody F126-2 against Ag84. Expression of $Ag84_{MS}$ from the acetamidase promoter without addition of the inducer acetamide was higher than wild-type expression levels (right panel). The sizes of molecular weight markers used for Western blots are indicated.

found in both phylogenetically distinct branches of gram-positive bacteria, firmicutes (low G+C content), and actinobacteria (high G+C content).

All *Mycobacterium* species whose genomes have been sequenced encode DivIVA orthologs (Fig. 1A). The *M. tuberculosis* ortholog has been identified as Ag84 (20, 27), which is encoded by the *wag31* (*Rv2145c*) gene (14). As shown for DivIVA in *B. subtilis*, Ag84 also displayed weak homology to

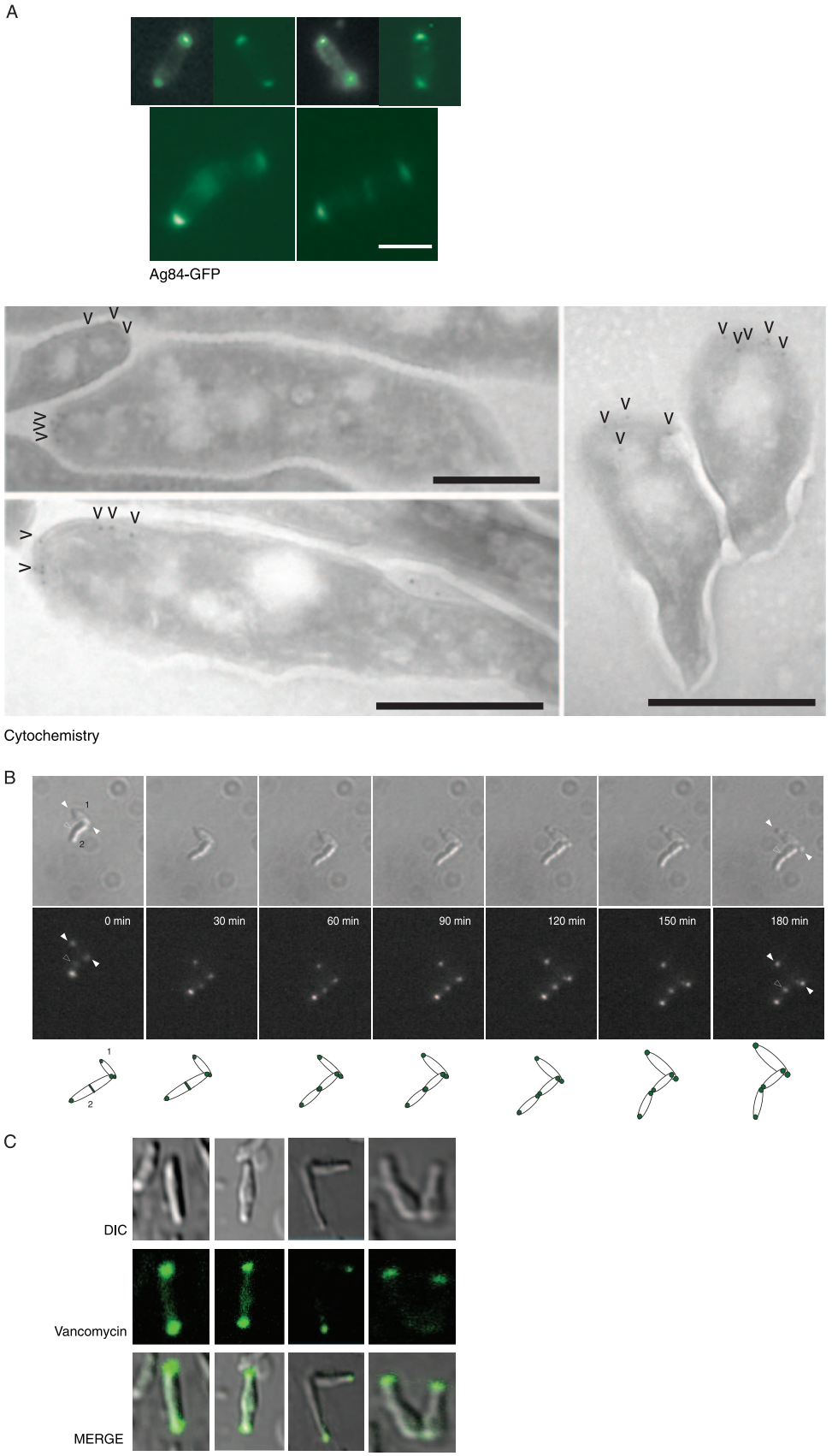

FIG. 2. $Ag84_{MS}$ is recruited to polar sites of cell wall extension during growth and to midcell during septation. Wild-type *M. smegmatis* cells were transformed with pNDL2, generating a mutation in which $wag31_{MS}$-GFP (encoding the $Ag84_{MS}$-GFP fusion protein) was expressed from its

proteins that play essential roles in morphogenesis of eukaryotic cells, e.g., tropomyosin CDC8 from fission yeast *Schizosaccharomyces pombe* (1, 25).

To study the function of Ag84, we attempted to delete the chromosomal *M. smegmatis wag31* gene by specialized transduction of wild-type *M. smegmatis* with a recombinant phage carrying a mutated locus (phNTL2111; Table 1). In this phage carrying the *wag31* locus, the structural gene was replaced by the hygromycin resistance gene. Transduction experiments using this Δ*wag31* phage resulted in the absence of hygromycin-resistant colonies, strongly suggesting that the gene was essential. This was supported by the fact that *wag31* disruption was made possible when wild-type *M. smegmatis wag31* was provided in *trans* with a vector carrying the gene expressed from an acetamide-inducible promoter, P_{ace} (pNDL5; Table 1) (Fig. 1B, left panel). Western blot analysis revealed that background expression from the P_{ace} promoter in the absence of the inducer acetamide was modestly (about twofold) higher than expression of *wag31* from its native promoter (Fig. 1B, right panel), thus effectively preventing protein depletion experiments.

The *Mycobacterium smegmatis* Ag84 homolog is found primarily at the polar sites of cell wall biosynthesis. To visually track Ag84 in *M. smegmatis*, a chimeric reporter protein was made by fusing the GFP to the C terminus of $Ag84_{MS}$. The gene encoding this hybrid protein (*wag31*$_{MS}$-*gfp*) was cloned into a suicide vector (pNDL2) which integrated into *M. smegmatis* chromosome and expressed $Ag84_{MS}$-GFP from the native *wag31* promoter. Fluorescence microscopic analyses revealed that the $Ag84_{MS}$-GFP fusion protein was localized at the cell poles (Fig. 2A, upper panels). Control experiments showed that localization was dependent on the presence of $Ag84_{MS}$, as native GFP protein (fused to seven amino acids of the heat shock protein in pMV361) was dispersed throughout the cells (not shown). Independent electron microscopic analysis using a monoclonal antibody raised against mycobacterial Ag84 (F126-2) (27) confirmed its polar localization (Fig. 2A, lower panels). To follow the dynamics of $Ag84_{MS}$-GFP localization, two asynchronous cells representing the entire division cycle were observed under the fluorescence microscope for 180 min. Time-lapse recording revealed that during cell wall extension, $Ag84_{MS}$ was localized to the pole (represented by cell 1 in Fig. 2B). In a cell representing later stages (cell 2) it also accumulated at the midcell and was associated by morphogenesis into a "V"-shaped predivisional cell (Fig. 2B) followed by cell division.

A fluorescent derivative of the peptidoglycan biosynthesis inhibitor vancomycin was used to determine whether cell wall assembly was associated with DivIVA accumulation (17). *M. smegmatis* wild-type cultures were grown for approximately one generation (2 to 3 h) in the presence of labeled vancomycin before visualization by fluorescence microscopy. Fluorescent vancomycin accumulated mainly at the poles, which suggested that cells grow by polar cell wall extension (Fig. 2C). While $Ag84_{MS}$ was found at the midcell of some elongating rods (Fig. 2A), vancomycin was not (Fig. 2C). Inspection of vancomycin-labeled "V"-shaped cells revealed cell wall biosynthesis at the "V" junction, corresponding to the new poles of the nascent daughter cells. Vancomycin labeling at midcell (12) and at the junction of "V"-shaped dividing cells (61) has been also observed by other groups.

Overexpression of Ag84 led to the formation of giant cells having branches and distorted shapes. Expression of $Ag84_{MS}$ from the strong promoter P_{hsp60} led to major changes in *M. smegmatis* size and morphology (Fig. 3 and 4). Cells overexpressing $Ag84_{MS}$ (pNDL4) (Fig. 3A and 5A), *M. tuberculosis* $Ag84_{TB}$ (pNDL8) (Fig. 5A), or the $Ag84_{MS}$-GFP fusion protein (pNDL1) (Fig. 3B, 3C, 4A, and 5A) were grossly enlarged and had a diverse array of shapes. Attempts to label these cultures with various concentrations of fluorescent vancomycin were unsuccessful; they were apparently more sensitive to this antibiotic. Cells growing on selective agar plates for 2 days following transformation had enlarged, bowling-pin-shaped morphologies and often formed branches (Fig. 3A, 3B, and 4). Visual inspection of cultures on day 3 showed that the grossly enlarged cells were replaced by a population of cells having different sizes and shapes (Fig. 3C). Cell size and shape in the population gradually became similar to that of the wild type by day 5 (Fig. 3D). To track these changes, width and length (Fig. 5A) were measured throughout growth in cells overexpressing various Ag84 alleles ($Ag84_{MS}$, $Ag84_{MS}$-GFP, or $Ag84_{TB}$). These studies showed that all overexpressed Ag84 alleles initially induced enormous increases in cell length and width which expanded cell volume up to 80-fold. The average size of the cells gradually decreased over the next 6 days, and eventually they were identical to the wild type in width (Fig. 5A, left panel) and length (Fig. 5A, right panel). Thus, a diverse array of morphological changes was observed in cells in response to the introduction of vectors overexpressing various Ag84 proteins. Attempts to obtain stable variant cultures were unsuccessful, as purified colonies were often composed of a spectrum of different cell morphologies.

Western blot analyses were carried out to determine whether the dramatic morphological changes might be ex-

native genomic promoter. Transformants grown on selective plates for 4 days were prepared for microscopic analyses. (A) Localization of Ag84. *M. smegmatis* cells expressing $Ag84_{MS}$-GFP (pNDL2) were photographed under a fluorescence microscope (upper panels). In the majority of cells, fluorescence was observed at the cell poles. In elongated cells, $Ag84_{MS}$-GFP was also detected at the midcell. Bar, 1 μm. Polar localization was also observed by TEM using a monoclonal antibody against Ag84 (lower panels) to visualize Ag84 in cross-sections of cells. Arrowheads indicate positions of gold particles. Bars in lower panels, 0.5 μm. (B) Time-lapse video microscopy of *Mycobacterium smegmatis* mc^2155 expressing *wag31*$_{MS\text{-}gfp}$ over a period of 180 min. A representative series of images of a cell size extension event (cell 1) and a cell division event (cell 2) viewed with differential interference contrast (DIC) (upper panels) and fluorescence (lower panels) microscopy are shown. Sites of extension and division are indicated by filled and empty arrows, respectively. Time points are indicated in minutes. Cartoon interpretations are shown below the panels. (C) Nascent peptidoglycan synthesis is localized at the poles, as revealed by staining growing cell walls with fluorescent vancomycin. *M. smegmatis* wild-type cells cultured on 7H10 agar medium for 4 days at 37°C were labeled and observed by use of a fluorescence microscope as described in Materials and Methods.

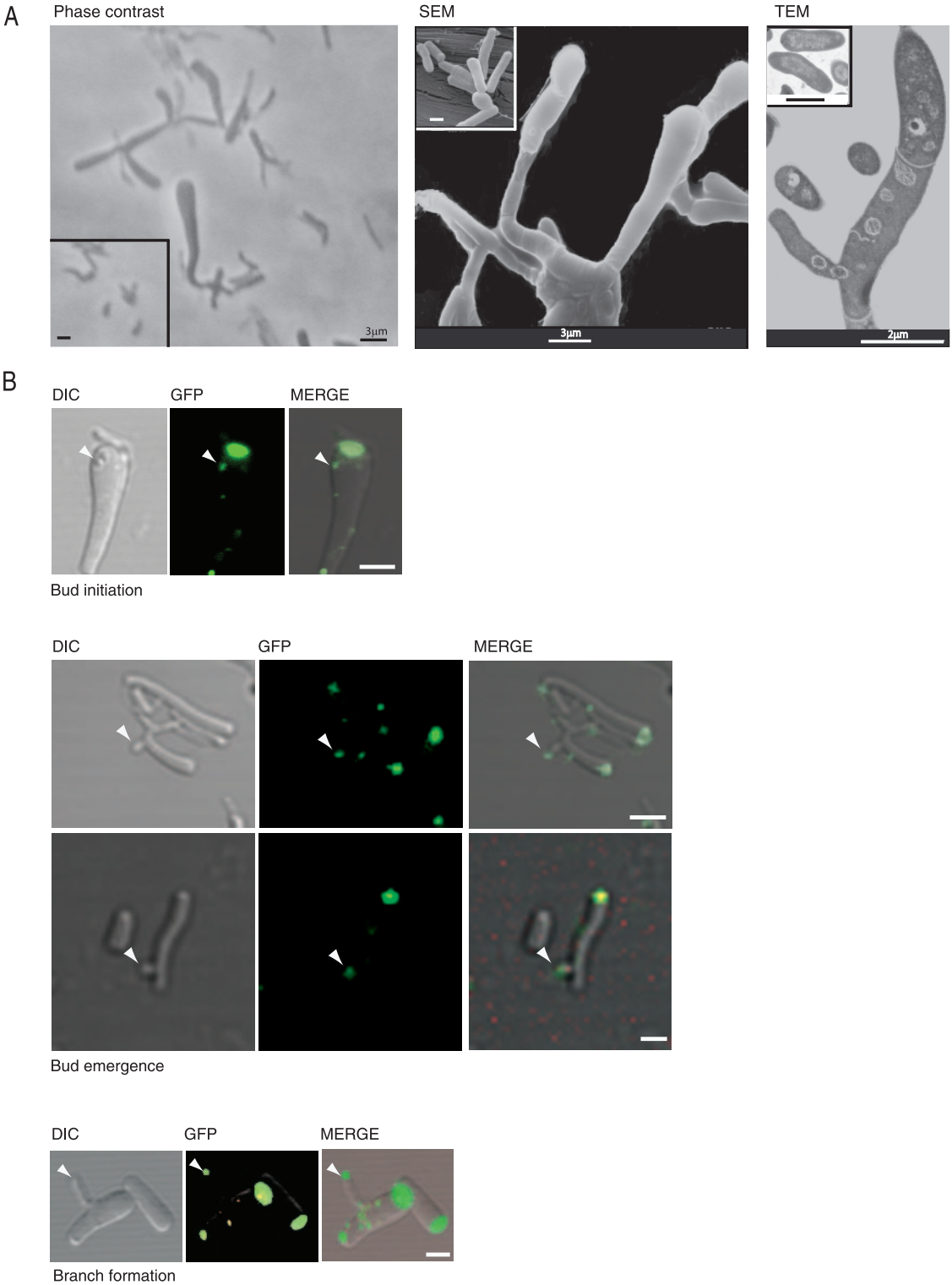

plained simply by the loss of the overexpressed $Ag84_{MS}$-GFP gene (Fig. 5C). Importantly, at least 95% of the cells observed microscopically retained $Ag84_{MS}$-GFP fluorescence. Transformed cultures were grown on selective agar plates and sampled daily. These blots recorded the amounts of both native $Ag84_{MS}$ and $Ag84_{MS}$-GFP for a period of 8 days. Indeed, the cloned $Ag84_{MS}$-GFP-encoding gene transcribed from P_{hsp60} provided levels of product about 2× to 3× higher than that seen with $Ag84_{MS}$ transcribed from its native promoter on day 1. By day 5, when cell size had reverted to that of the wild type

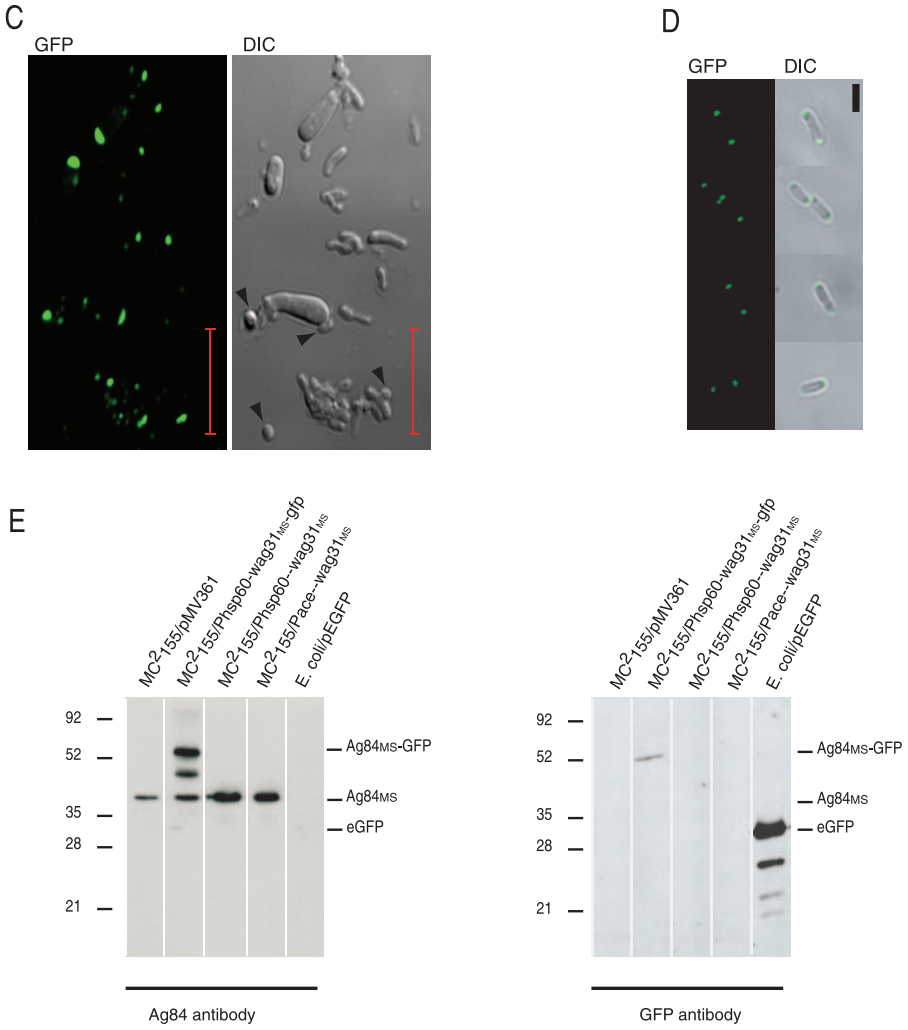

FIG. 3. Overexpression of *wag31*$_{MS}$ altered the morphology of *M. smegmatis* cells. Wild-type *M. smegmatis* cells were transformed with pNDL4 overexpressing *wag31*$_{MS}$ or with pNDL1 in which the *wag31*$_{MS}$*-gfp* (encoding the Ag84$_{MS}$-GFP fusion protein) was overexpressed from P$_{hsp60}$. (A) Enlargement and branching of *M. smegmatis* overexpressing *wag31*$_{MS}$ (pNDL4). After 2 days of growth on selective medium, transformants were harvested and observed. Left, middle, and right panels show phase-contrast, scanning electron microscopy (SEM), and TEM images of *M. smegmatis* overexpressing *wag31*$_{MS}$. Insets: left panel, wild-type *M. smegmatis* mc^{2}155 as control (bar in the inset, 1 μm); middle panel, relative shape and size of wild-type *M. smegmatis* mc^{2}155 (bar in the inset, 0.5 μm); right panel, wild-type *M. smegmatis* mc^{2}155 as control (bar in the inset, 0.91 μm). (B) Accumulations of Ag84$_{MS}$-GFP (pNDL1) along the cylindrical part of cells were often associated with bud initiation (white arrows, top panels). Later, structures resembling emerging buds contained localized patches of Ag84$_{MS}$ (white arrows, middle panels). Emerging branches contained Ag84$_{MS}$ at the growing tip (white arrows, bottom panels). Bars, 3 μm. (C) Distorted heterogeneous shapes of *M. smegmatis* overexpressing *wag31*$_{MS}$*-gfp* (pNDL1). After 3 days of growth on selective medium, transformants were viewed using differential interference contrast (DIC) and fluorescence modes. Similar results were obtained with cells overexpressing *wag31*$_{MS}$ alone. Minicells (arrows) and cells having rod, ovoid, round, or bottle-like shapes were observed. DAPI (4′,6′-diamidino-2-phenylindole) staining experiments showed that the majority of these small cells did not have DNA (data not shown). Bars, 10 μm. (D) By day 5 after transformation, *M. smegmatis* cells transformed with the *wag31*$_{MS}$*-gfp*-overexpressing plasmid exhibited normal size and morphology. Bar, 2 μm. (E) Expression of Ag84$_{MS}$ in cell extracts of *M. smegmatis* strains cultured on 7H10 agar plates for 3 days at 37°C was detected by Western blot analysis with antibody against antigen 84 (F126-2; left panel) or GFP (right panel). The middle band in mc^{2}155/P$_{hsp60}$-*wag31*$_{MS}$*-gfp* most likely represents a GFP degradation product of Ag84$_{MS}$-GFP. The sizes of molecular weight markers used for Western blots are indicated.

(Fig. 5) in roughly 90% of the transformants, the amount of Ag84$_{MS}$-GFP decreased by about 50%.

These unusual morphologies during early growth of overexpressing strains were associated with localized accumulations of Ag84$_{MS}$-GFP. In the giant, bowling pin-shaped cells, Ag84$_{MS}$-GFP was distributed asymmetrically at the enlarged pole, suggesting that Ag84$_{MS}$ influenced polar cell wall extension and affected both length and diameter (Fig. 4A). Regions adjacent to these Ag84$_{MS}$-GFP accumulations did not contain septa that could be detected using the membrane stain FM4-64. Interestingly, septa were formed at the narrow poles that contained less Ag84$_{MS}$ (Fig. 4A and B). As the average cell of the population became progressively smaller and symmetric with time of incubation, the intensity of Ag84-GFP per cell decreased and became more equally distributed between the poles. While only about 2% of the cells had a symmetric dis-

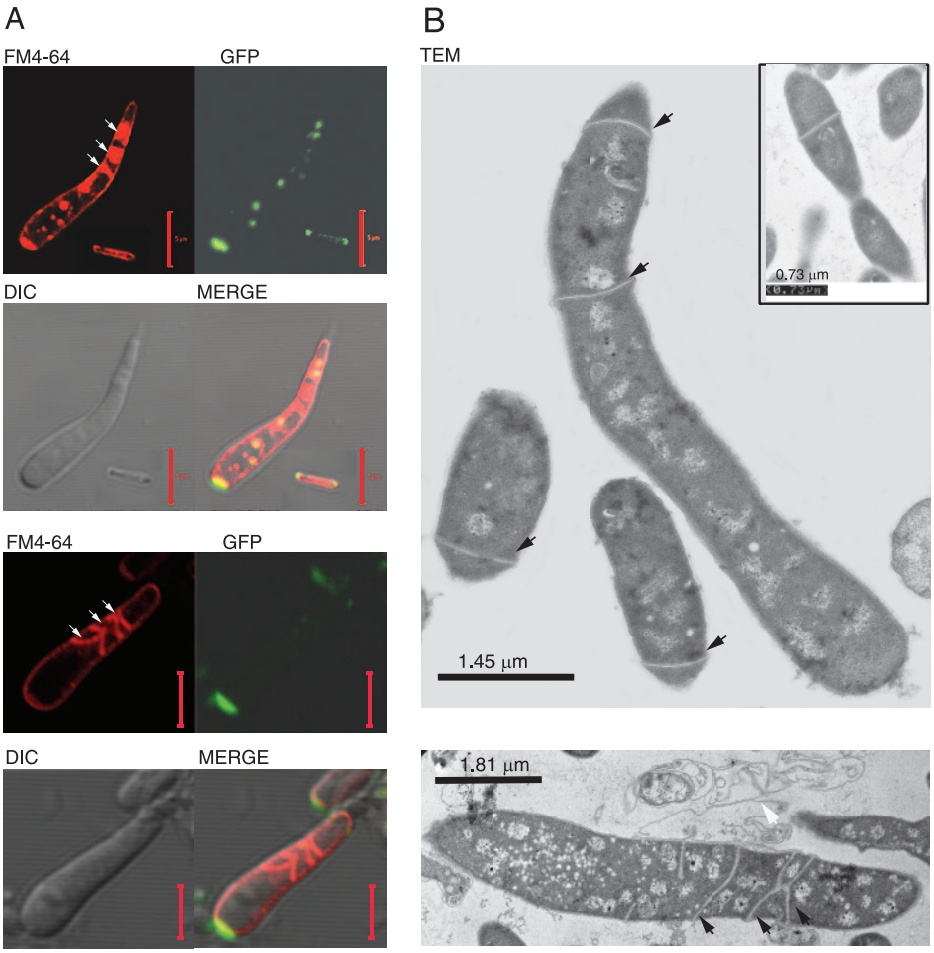

FIG. 4. $Ag84_{MS}$ overexpression inhibited septum formation and created giant cells. (A) Giant cells overexpressing *wag31*$_{MS}$-*gfp* from the heat shock promoter P_{hsp60}. Cell volume increased up to 80-fold. The wild-type cell at the bottom right corner (top panels) displays normal shape and size. Bar, 5 μm. Membranes were stained red with FM4-64. Arrows show the accumulation of septum formation at the narrow end of the cell where Ag84-GFP was not accumulated. (B) Transmission electron microscopic images of a giant cell and of wild-type cells. Black arrows show sites of asymmetric septation. Abnormal septation also created polar anuclear compartments. Lysed ghost cells were also observed (white arrow).

tribution of Ag84-GFP after 2 days of growth, by 5 days, >95% of the cells had symmetric distributions indistinguishable from those of the wild type (Fig. 3D and 5B).

Other morphological shape distortions were observed in the giant cells after 2 to 3 days of growth; examples are displayed in Fig. 3B. In addition to its predominant polar localization, $Ag84_{MS}$-GFP was also observed adjacent to unusual circular structures along the surface of the cylindrical part of the cell wall; these structures are likely to have represented the earliest visible stage of bud initiation (Fig. 3B, top panels). Extensions resembling emerging buds also contained localized patches of $Ag84_{MS}$-GFP (Fig. 3B, middle panels). More extended branches contained $Ag84_{MS}$-GFP at the growing tip (Fig. 3B, bottom panels).

Oligomerization of Ag84. Cell fractionation and Western blot analyses using monoclonal antibodies revealed that $Ag84_{MS}$ was present in the *M. smegmatis* cytoplasm but not present in the membrane fraction (Fig. 6A). This suggested that its polar localization was not determined by strong hydrophobic interactions with the membrane. Instead, polar localization may be a consequence of the three-dimensional shape of DivIVA multimers that fit into the curvature of the pole (20).

Bioinformatic analyses (MultiCoil program; 67) comparing *B. subtilis* DivIVA to mycobacterial Ag84 protein sequences predicted two coiled-coil domains that might catalyze polymerization (Fig. 6B). In the 164-amino-acid *B. subtilis* DivIVA sequence, the two predicted coiled-coil domains extended over most of the protein, excluding the intercoil region and both termini. Both coiled-coil domains were predicted to be dimeric. In contrast, the mycobacterial Ag84 proteins were much longer (260 amino acids in *M. tuberculosis* and 272 amino acids in *M. smegmatis*), having additional amino acids within both the intercoil region and the second coiled-coil domain. This intercoil region included a phosphorylation site (T73) that is necessary for Ag84 activity (31). Finally, Ag84 proteins were different from the *B. subtilis* ortholog in that their C-terminal coiled-coil structure was predicted to be trimeric rather than dimeric.

To test whether Ag84 was oligomerized in vivo, cell extract of wild-type *M. bovis* BCG was treated with different concen-

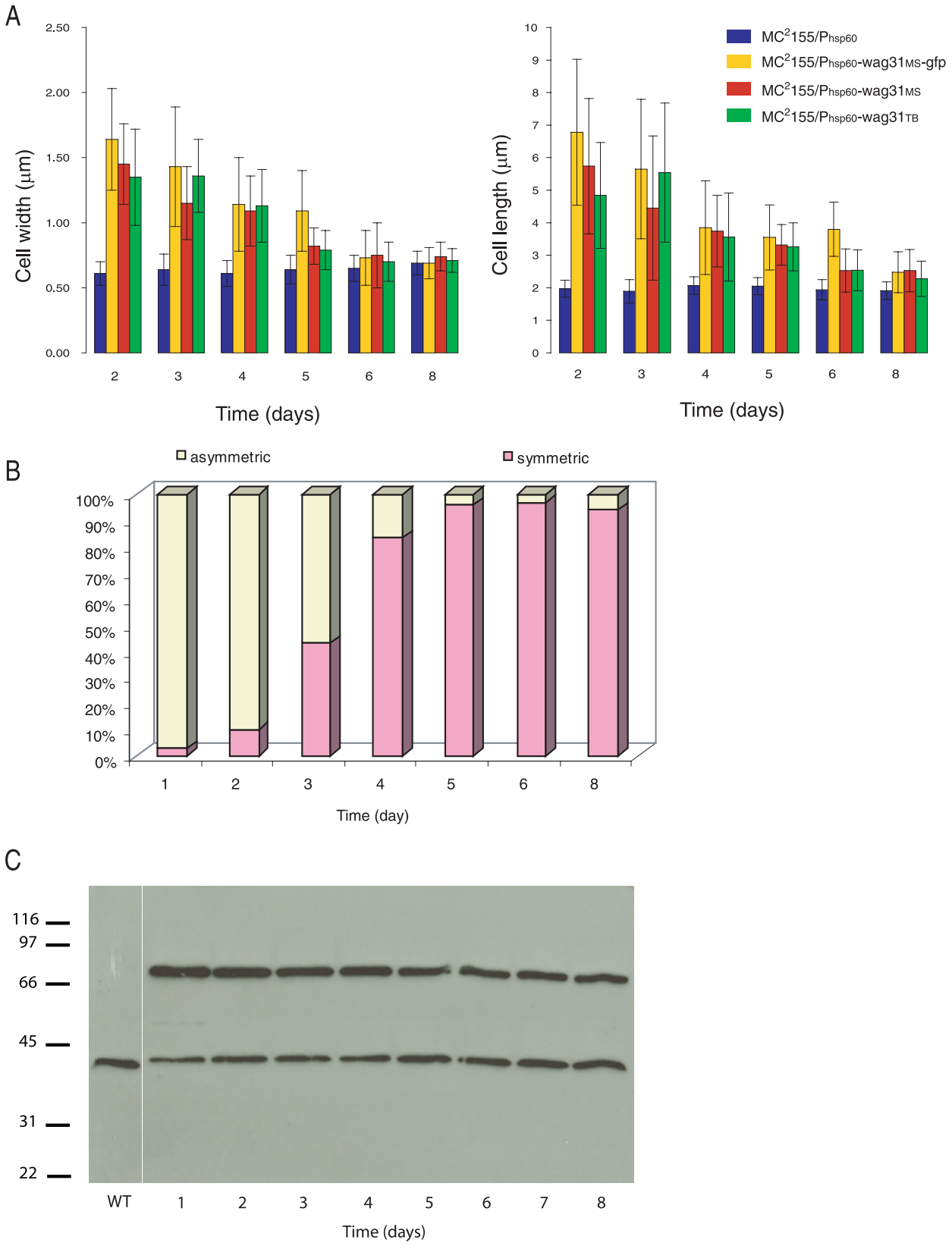

FIG. 5. Cell size and shape in *M. smegmatis* mc^{2}155 are dependent on levels of Ag84 expression. Bacteria from colonies grown on agar plates at 37°C were resuspended in liquid medium and diluted to a density of 10 to 20 cells per microscopic focal plane. (A) Mean values of cell lengths and widths of *M. smegmatis* mc^{2}155 cells measured at interval time points (days) after transformation with pMV361 (blue), pNDL1 (yellow), pNDL4 (red), and pNDL8 (green). Cell length and width were measured as described in Materials and Methods. Error bars represent standard deviation of the mean ($n \sim 100$ cells per strain). (B) Time-dependent symmetric versus asymmetric localization of Ag84 in *M. smegmatis* mc^{2}155 cells overexpressing $Ag84_{MS}$-GFP. (C) Kinetics of Ag84 overexpression associated with induced changes in cell morphology. *M. smegmatis* was transformed with pNDL1 and plated on agar plates at 37°C. Cell extracts were prepared daily from cells grown on agar plates and analyzed using Western blots and F126-2 antibody.

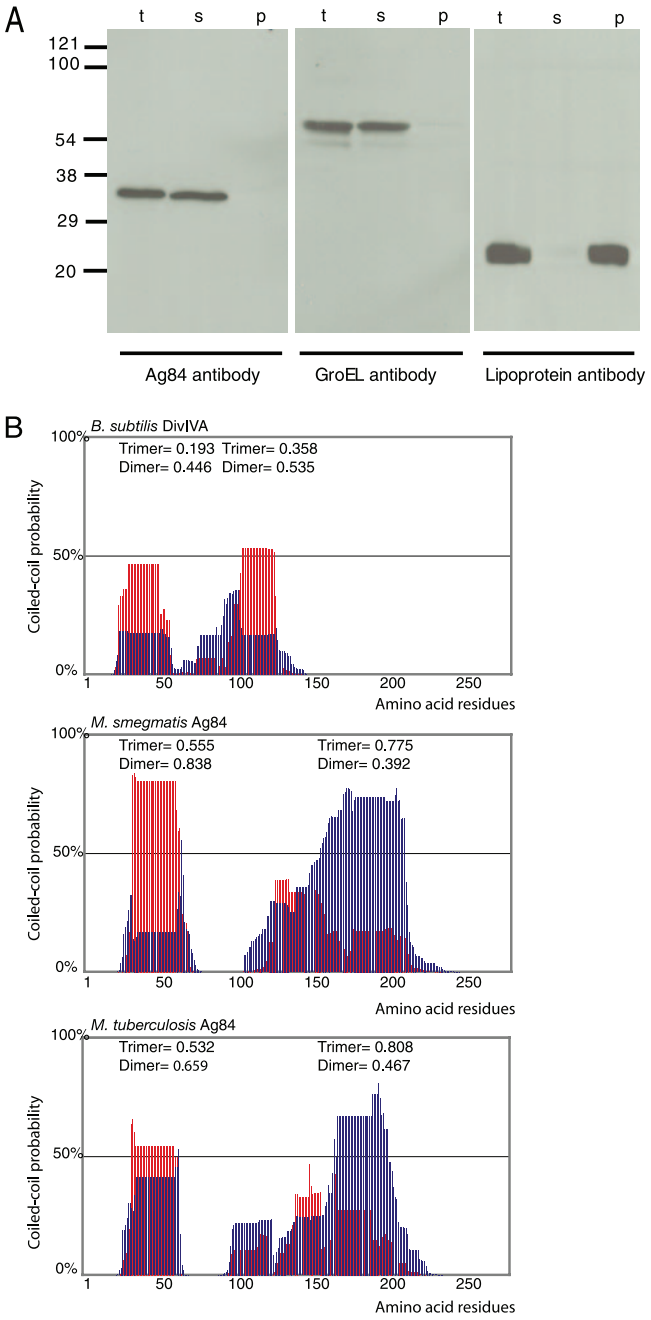

FIG. 6. Oligomerization of mycobacterial antigen 84. (A) Subcellular localization of Ag84 in *M. bovis* BCG lysates. Bacterial cultures were grown at 37°C in 7H9-OADC medium, and cellular fractionation was carried out as described in Materials and Methods. Ag84 was detected in subcellular fractions by Western blot analysis using F126-2 antibody. GroEL- and lipoprotein-specific antibodies were used as controls for cytosolic and membrane proteins, respectively (t, total cell extract; s, supernatant; p, pellet). (B) Prediction of coiled-coil domains in DivIVA and Ag84 proteins. Protein sequences were analyzed with the MultiCoil (67) parallel coiled-coil prediction algorithm, using a 0.5 cutoff for the maximum scoring residue. The graphs show the calculated probabilities (*y* axis) for trimeric (blue bars) and dimeric (red bars) coiled coils versus the amino acid residue position (*x* axis). The overall probability of a coiled-coil domain is divided into a dimeric and a trimeric portion (values indicated above each domain). (C) Cross-linking of *M. bovis* BCG Ag84 in cell extracts (upper left panel) and purified *M. bovis* BCG Ag84 protein (upper right panel) by incubation with different concentrations (0.1 to 2%) of formaldehyde followed by SDS-PAGE and immunoblotting to detect mono- and oligomers with Ag84-specific F126-2 antibody. A lipoprotein-specific antibody was used as a control (lower panel). (D) Size-exclusion chromatography to analyze the molecular weight of Ag84 oligomers. Cell lysate of *M. bovis* BCG was applied to a gel filtration column equilibrated in PBS, and fractions were collected. Values representing elution of protein standards are indicated above the chromatogram. (E) Aliquots of the fractions indicated were loaded on 12.5% SDS gels and analyzed for the presence of Ag84 by Western blotting. Ag84 was detected in a single fraction that corresponded to a molecular weight of ~670. The sizes of molecular weight markers used for Western blots (A, C, and E) or gel filtration (D) are indicated.

trations of the cross-linking agent formaldehyde and analyzed on Western blots. Increased concentrations of formaldehyde resulted in incremental mobility shifts of a protein that cross-reacted with the Ag84 antibody (Fig. 6C, top left panel). The sizes of these shifted bands corresponded roughly to those of homodimers, homotetramers, and homohexamers of Ag84; higher-order oligomers might also be present but were not resolved by SDS-PAGE. To confirm oligomerization, Ag84 was purified from *M. bovis* BCG extracts by affinity chromatography using F126-2 antibody, treated with formaldehyde, and analyzed as described above for *M. bovis* BCG extracts. Cross-linking of this purified Ag84 displayed a similar polymerization pattern, suggesting that homo-oligomerization is a characteristic of the protein in vivo (Fig. 6C, top right panel). In control experiments, detection of a lipoprotein in the cross-linked cell extract did not show a comparable oligomerization pattern (Fig. 6C, bottom panel).

To determine the molecular weight of Ag84 oligomers in the cytoplasm, cell lysate of *M. bovis* BCG was separated on a gel filtration column (Fig. 6D) and Ag84 was detected in the fractions using Western blotting (Fig. 6E). Ag84 was found in a single fraction, and, based on the comparison with protein standards, its molecular weight was estimated to be around 670 (Fig. 6D and 6E).

DISCUSSION

While common principles have emerged in our understanding of how cell shape is determined in various bacterial genera, which proteins are used and how they work together may be a function of the characteristic shape and phylogeny of the individual bacterium. Here we show that *M. smegmatis*, which lacks many proteins essential for growth and division in other bacteria, requires Ag84, a protein that is absent in many bacterial genera. Overexpression experiments indicated that DivIVA is involved in morphogenesis functions, including growth and cell division. These processes may require specialized mechanisms in mycobacteria, allowing them to remodel their multilayered cell envelope. Unlike *B. subtilis* and most other gram-positive bacteria, many actinomycetes have cell walls that contain not one but at least three distinct layers (peptidoglycan, arabinogalactan, and mycolic acid [18, 39]) whose sizes and shapes must be closely matched to avoid cell distortion (15). While cell wall biosynthesis may occur at multiple sites within the cylindrical body of many bacteria, localized biosynthetic centers might facilitate coordinated assembly

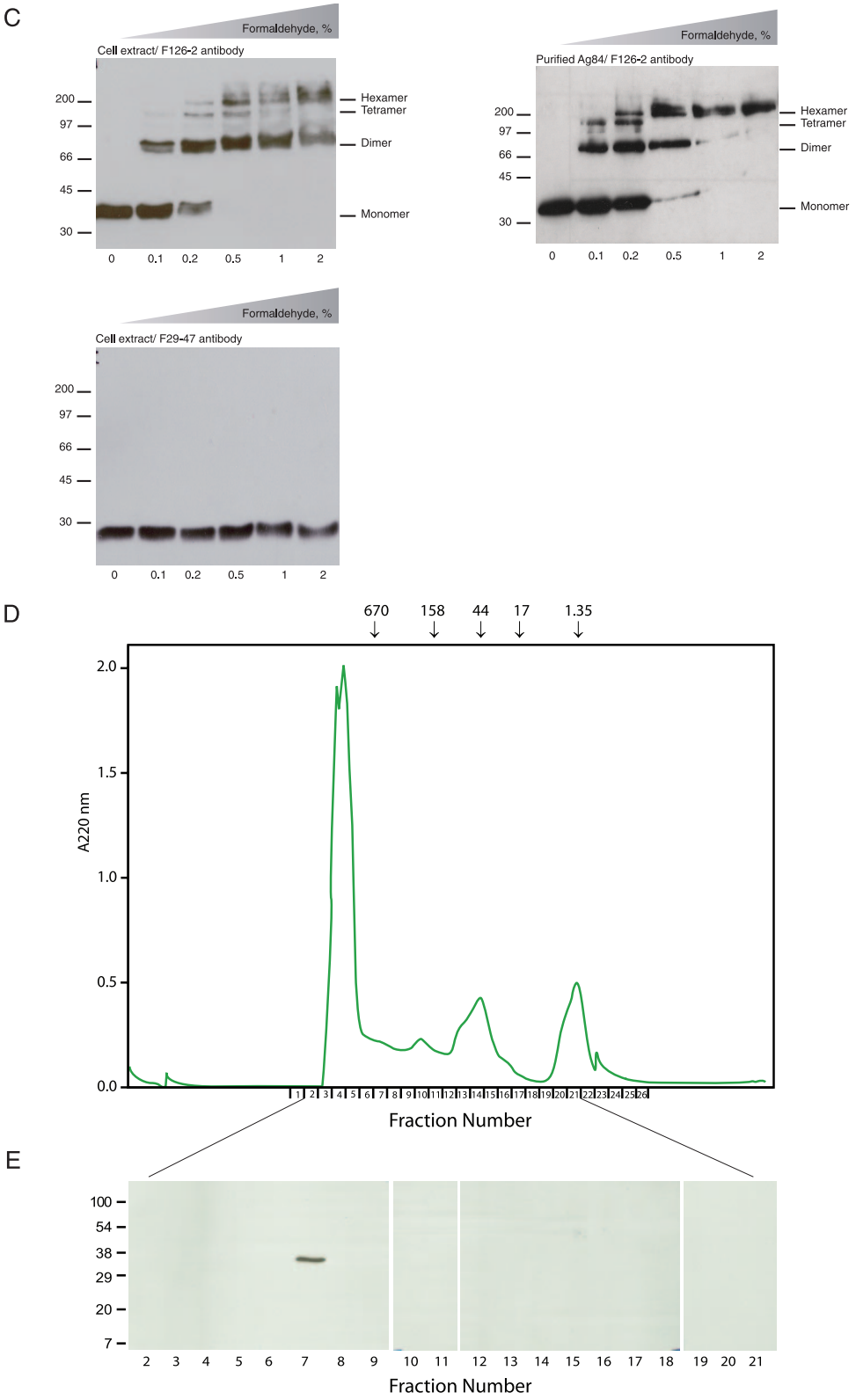

FIG. 6—*Continued.*

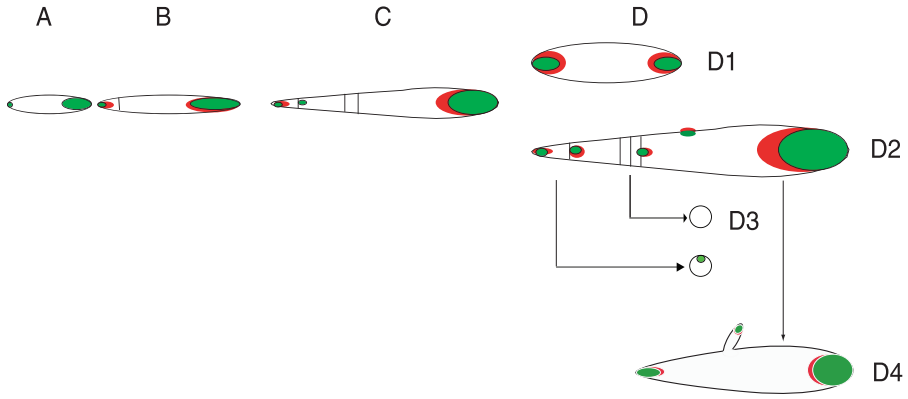

FIG. 7. A model rationalizing how overexpression of Ag84 in *M. smegmatis* results in pleiomorphism in a subpopulation of cells. Overexpressed Ag84 (green) progressively accumulates at one pole (A and B). This results in cell wall expansion (red) and a localized increase in cell diameter at one pole, with septation observed at the opposite pole (C). This creates bowling-pin-shaped giant cells (D2) and small cells (D3; see Fig. 3C). Alternatively, a recovery in balanced distribution of DivIVA creates rod-shaped giant cells (D1). Untargeted accumulation of Ag84 along the lateral cell wall stimulates cell wall expansion leading to the formation of branches (D4).

of a cross-linked multilayered cell envelope, thus allowing the subsequent evolution of a complex cell wall in actinomycetes species.

The phenotypes of *M. smegmatis* $Ag84_{MS}$-overexpressing cells predict central functions in growth and division. While Ag84 was found equally distributed at the poles in wild-type cells (Fig. 2A and 2B [cell 1]), when overexpressed, large amounts of $Ag84_{MS}$ accumulated at one pole, resulting in progressive localized phenotypic effects (Fig. 3 and 4). These effects were observed early after transformation; cell wall material and ghosts eventually appeared in the medium, and extensive lysis was apparently taking place. To rationalize the observed effects of overexpression on a subpopulation of cells, we propose the model shown in Fig. 7. In response to overexpression, and perhaps according to dependence on specific growth or nutritional conditions, cell wall biosynthesis increases at the $Ag84_{MS}$-containing pole (Fig. 7B and C) whereas the formation (or maintenance) of stable new septa was not observed (Fig. 7C). By analogy to those of other rod-shaped bacteria, these two peptidoglycan biosynthetic processes may involve mutually exclusive enzymatic activities that determine length or width (34) and $Ag84_{MS}$ may exert this effect on morphology by inhibiting systems for septum formation or promoting polar sites involved with lateral cell wall extension. However, the coordinated effects of overexpression on both length and width near the pole suggest a more interactive system in these pleiomorphic actinobacteria. Overexpression may reflect simultaneous activation of multiple cell wall biosynthetic systems at this polar site. It is also possible that the switch to septum formation cannot take place after the diameter of the cell exceeds a certain limit, thus leading to an irreversible expansion of the pole. Discrete localized foci of Ag84 were also present at buds and emerging branches. Small, minicell-like structures were observed. Electron microscopic observations (15) have suggested that *M. tuberculosis* can indeed produce minicell-like structures as shown in the model (see D3 in Fig. 7). Overexpression eventually generated a heterogeneous population of enlarged polymorphic cells (Fig. 7D). It is likely that such cells undergo lysis, as has been described for *S. coelicolor* (22).

By day 5 after transformation, cells in the culture become more like the wild type in size and shape, with Ag84-GFP symmetrically distributed at the poles. Western blot analyses (Fig. 5C) showed that the reduction of average cell size was not accompanied by a proportional reduction in the levels of Ag84-GFP protein that induced the changes. This, along with retention of the GFP fluorescence in surviving cells, showed that progressive loss of Ag84 activity did not account for reversion of the phenotype in the culture. We consider it unlikely that a population of independent suppressor mutations overtook a growth-arrested population of primary transformants because of the frequency at which it occurred. We routinely generate fewer than 10,000 primary transformants, and rates of spontaneous mutagenesis allowing growth would not be able to generate the semiconfluent growth over the surface of the plate that was observed. Furthermore, enlarged cells having aberrant morphologies were retained in colonies purified from these cultures. While we cannot formally rule out the possibility that restoration of the wild-type morphology might represent unlinked genomic suppressor mutations, we believe that progressive physiological changes took place in the culture to adjust to Ag84 overexpression and that these changes were accompanied, or perhaps caused by, a decrease in the levels of P_{hsp60}-driven expression of Ag84-GFP.

Based on these observations and what is known about DivIVA in *B. subtilis*, we can rationalize how rod-like *Mycobacterium* species use Ag84 to achieve and maintain their elongated shape during normal growth and cell division. Elongation of cells is associated with peptidoglycan biosynthesis, and Ag84 is distributed equally at the cell poles (Fig. 2B, cell 1). This might inhibit septum formation near the poles during elongation. Ag84 appeared at the midcell in elongated straight cells (Fig. 2B, cell 2) before vancomycin staining became evident. This may indicate that the peptidoglycan biosynthetic machinery that closes the septum arrives at midcell after Ag84; however, this is apparently not the case in *B. subtilis* (36, 37). It is also possible that the nature of the peptidoglycan peptide side chains at the septum site means that they may not bind vancomycin as well or that the midcell section of the envelope is intrinsically less permeable to vancomycin. Detailed kinetic

and genetic analyses such as those carried out with *B. subtilis* (26, 36, 37) will be needed to determine the order of assembly of Ag84 and peptidoglycan biosynthetic enzymes at the midcell. Subsequent asymmetric growth of the septum might initially bend the predivisional cell (Fig. 2B, cell 2), culminating in closure of the septum to generate the daughter cells. Our observations are consistent with reports of polar vancomycin labeling in *Corynebacterium glutamicum* (17) and *Streptomyces coelicolor* (22, 23), supporting the model for rod-shaped bacterial morphogenesis originally proposed by Daniel and Errington (17).

As with DivIVA in *B. subtilis*, Ag84 was present at the poles in virtually all cells, perhaps localized by a characteristic superstructure (20, 58). In vitro cross-linking experiments provided evidence that Ag84 formed homo-oligomers in the cytoplasm of mycobacteria. Similar oligomerized forms of *B. subtilis* DivIVA (40, 58) serve as building blocks for the formation of two-dimensional lattices. These structures may help DivIVA/Ag84 recognize general features of the cell poles (20, 26, 58). This idea is supported by the observation that the *B. subtilis* DivIVA protein can recognize poles of *E. coli* and *Schizosaccharomyces pombe* cells that do not have DivIVA genes (20). However, it does not explain its ability to induce branching from tubular surfaces of the *M. smegmatis* cell wall.

The possibility that mycobacterial Ag84 has some unique biophysical properties (20) or polymerization properties (58) as reported for *B. subtilis* DivIVA was supported by sequence analysis. Coiled-coil structures, a common protein fold motif, are composed of two or more alpha helices wound around one another. The coiled-coil fold serves as "molecular Velcro" to stabilize protein tertiary-structures or higher-order assemblies of proteins, often at membrane interfaces (49). Our biochemical data demonstrating homo-oligomerization of Ag84 (Fig. 6) are consistent with those observed for *B. subtilis* DivIVA; however, its quaternary structure and interactive heterologous partners are not likely to be the same. The sequence divergence between Ag84 and DivIVA in the intercoil region may serve as a target for alternative interactive partners that may have lesser affinity or may not be present at stoichiometry concentrations. For example, the enzyme PknA phosphorylates a threonine residue (T73) (31) in this region. Sequence analyses indicate that Ag84 may form not only dimeric but also trimeric folds (Fig. 6B). This trimeric fold may provide for an alternative form of the tertiary structure of the protein or its higher-order superstructure. The suggestion that DivIVA may have species-specific shapes or partners is supported by studies of the *Enterococcus faecalis* DivIVA showing that it is not functional in *B. subtilis* or *Streptococcus pneumoniae* (46).

While we observed morphologies for *M. smegmatis* that do not occur under laboratory culture conditions, some have been observed for related *Mycobacterium* and *Streptomyces* species. *M. tuberculosis* cells are rather polymorphic (15), and their morphology changes during persistence in lungs as well as starvation in vitro (53, 56). Interestingly, when grown in macrophages, *M. tuberculosis* becomes filamentous and contains spiral-like FtsZ structures throughout the length of the cell (13). In addition, many *Mycobacterium* species are reported to become shorter, spherical, ovoid, filamentous, or branching, depending on the physiological state (44, 53, 56, 61). Polymorphism has also been described in other rod-like actinobacteria such as *Rhodococcus*, *Arthrobacter*, *Corynebacterium*, and *Nocardia* species. Morphological changes due to overexpression of a DivIVA homolog have been reported for the polymorphic *Brevibacterium* species (47). Finally, cell branching, similar to that induced by $Ag84_{MS}$ overexpression in *M. smegmatis*, is a characteristic of *Streptomyces* species. Thus, it is interesting to speculate that the diverse morphologies of actinomycetes might be a function of their different systems to regulate the activity or localization of DivIVA homologs. If so, actinobacteria may regulate concentration or spatial localization of DivIVA homologs to adjust their shapes or sizes, effectively altering their volume-to-surface area. Such changes might accommodate changes in uptake and metabolic flux in response to altered environments (13).

ACKNOWLEDGMENTS

We thank William R. Jacobs, Jr., Brigitte Gicquel, and Arend Kolk for providing mycobacterial plasmids, strains, and antibodies used in this work, Danielle Ringoir for technical assistance, and Daniel Mathys, Ursula Sauder, and Cristina Prescianotto-Baschong for electron microscopic analyses. Preliminary sequence data of *M. smegmatis* were obtained from The Institute for Genomic Research through the website at http://www.tigr.org.

This work was supported by Swiss National Science Foundation grants to C.J.T. and J.P., a Canadian Natural Science and Engineering Research Council grant to C.J.T. (293171-06), a World Health Organization grant to J.P., and startup funds from the Case Western Reserve University School of Medicine to L.N.

REFERENCES

1. **Balasubramanian, M. K., D. M. Helfman, and S. M. Hemmingsen.** 1992. A new tropomyosin essential for cytokinesis in the fission yeast *S. pombe*. Nature **360:**84–87.
2. **Balasubramanian, V., M. S. Pavelka, Jr., S. S. Bardarov, J. Martin, T. R. Weisbrod, R. A. McAdam, B. R. Bloom, and W. R. Jacobs, Jr.** 1996. Allelic exchange in *Mycobacterium tuberculosis* with long linear recombination substrates. J. Bacteriol. **178:**273–279.
3. **Bardarov, S., S. Bardarov, Jr., M. S. Pavelka, Jr., V. Sambandamurthy, M. Larsen, J. Tufariello, J. Chan, G. Hatfull, and W. R. Jacobs, Jr.** 2002. Specialized transduction: an efficient method for generating marked and unmarked targeted gene disruptions in *Mycobacterium tuberculosis*, *M. bovis* BCG and *M. smegmatis*. Microbiology **148:**3007–3017.
4. **Bernhardt, T. G., and P. A. de Boer.** 2005. SlmA, a nucleoid-associated, FtsZ binding protein required for blocking septal ring assembly over chromosomes in *E. coli*. Mol. Cell **18:**555–564.
5. **Burnette, W. N.** 1981. "Western blotting": electrophoretic transfer of proteins from sodium dodecyl sulfate-polyacrylamide gels to unmodified nitrocellulose and radiographic detection with antibody and radioiodinated protein A. Anal. Biochem. **112:**195–203.
6. **Cabeen, M. T., and C. Jacobs-Wagner.** 2005. Bacterial cell shape. Nat. Rev. Microbiol. **3:**601–610.
7. **Carballido-López, R.** 2006. Orchestrating bacterial cell morphogenesis. Mol. Microbiol. **60:**815–819.
8. **Carballido-López, R.** 2006. The bacterial actin-like cytoskeleton. Microbiol. Mol. Biol. Rev. **70:**888–909.
9. **Carballido-López, R., and J. Errington.** 2003. The bacterial cytoskeleton: in vivo dynamics of the actin-like protein Mbl of *Bacillus subtilis*. Dev. Cell **4:**19–28.
10. **Carriere, C., P. F. Riska, O. Zimhony, J. Kriakov, S. Bardarov, J. Burns, J. Chan, and W. R. Jacobs, Jr.** 1997. Conditionally replicating luciferase reporter phages: improved sensitivity for rapid detection and assessment of drug susceptibility of *Mycobacterium tuberculosis*. J. Clin. Microbiol. **35:** 3232–3239.
11. **Cha, J. H., and G. C. Stewart.** 1997. The *divIVA* minicell locus of *Bacillus subtilis*. J. Bacteriol. **179:**1671–1683.
12. **Chauhan, A., H. Lofton, E. Maloney, J. Moore, M. Fol, M. V. Madiraju, and M. Rajagopalan.** 2006. Interference of *Mycobacterium tuberculosis* cell division by Rv2719c, a cell wall hydrolase. Mol. Microbiol. **62:**132–147.
13. **Chauhan, A., M. V. Madiraju, M. Fol, H. Lofton, E. Maloney, R. Reynolds, and M. Rajagopalan.** 2006. *Mycobacterium tuberculosis* cells growing in macrophages are filamentous and deficient in FtsZ rings. J. Bacteriol. **188:**1856–1865.
14. **Cole, S. T., R. Brosch, J. Parkhill, T. Garnier, C. Churcher, D. Harris, S. V. Gordon, K. Eiglmeier, S. Gas, C. E. Barry 3rd, F. Tekaia, K. Badcock, D.**

Basham, D. Brown, T. Chillingworth, R. Connor, R. Davies, K. Devlin, T. Feltwell, S. Gentles, N. Hamlin, S. Holroyd, T. Hornsby, K. Jagels, B. G. Barrell, et al. 1998. Deciphering the biology of *Mycobacterium tuberculosis* from the complete genome sequence. Nature **393:**537–544.
15. **Dahl, J. L.** 2004. Electron microscopy analysis of *Mycobacterium tuberculosis* cell division. FEMS Microbiol. Lett. **240:**15–20.
16. **Dahl, J. L.** 2005. Scanning electron microscopy analysis of aged *Mycobacterium tuberculosis* cells. Can. J. Microbiol. **51:**277–281.
17. **Daniel, R. A., and J. Errington.** 2003. Control of cell morphogenesis in bacteria: two distinct ways to make a rod-shaped cell. Cell **113:**767–776.
18. **Dmitriev, B. A., S. Ehlers, E. T. Rietschel, and P. J. Brennan.** 2000. Molecular mechanics of the mycobacterial cell wall: from horizontal layers to vertical scaffolds. Int. J. Med. Microbiol. **290:**251–258.
19. **Edwards, D. H., and J. Errington.** 1997. The *Bacillus subtilis* DivIVA protein targets to the division septum and controls the site specificity of cell division. Mol. Microbiol. **24:**905–915.
20. **Edwards, D. H., H. B. Thomaides, and J. Errington.** 2000. Promiscuous targeting of *Bacillus subtilis* cell division protein DivIVA to division sites in *Escherichia coli* and fission yeast. EMBO J. **19:**2719–2727.
21. **Egelman, E. H.** 2003. Actin's prokaryotic homologs. Curr. Opin. Struct. Biol. **13:**244–248.
22. **Flärdh, K.** 2003. Essential role of DivIVA in polar growth and morphogenesis in *Streptomyces coelicolor* A3(2). Mol. Microbiol. **49:**1523–1536.
23. **Flärdh, K.** 2003. Growth polarity and cell division in *Streptomyces*. Curr. Opin. Microbiol. **6:**564–571.
24. **Goehring, N. W., and J. Beckwith.** 2005. Diverse paths to midcell: assembly of the bacterial cell division machinery. Curr. Biol. **15:**R514–R526.
25. **Gunning, P., R. Weinberger, and P. Jeffrey.** 1997. Actin and tropomyosin isoforms in morphogenesis. Anat. Embryol. (Berlin) **195:**311–315. (In German.)
26. **Harry, E. J., and P. J. Lewis.** 2003. Early targeting of Min proteins to the cell poles in germinated spores of *Bacillus subtilis*: evidence for division apparatus-independent recruitment of Min proteins to the division site. Mol. Microbiol. **47:**37–48.
27. **Hermans, P. W., F. Abebe, V. I. Kuteyi, A. H. Kolk, J. E. Thole, and M. Harboe.** 1995. Molecular and immunological characterization of the highly conserved antigen 84 from *Mycobacterium tuberculosis* and *Mycobacterium leprae*. Infect. Immun. **63:**954–960.
28. **Höltje, J. V.** 1998. Growth of the stress-bearing and shape-maintaining murein sacculus of *Escherichia coli*. Microbiol. Mol. Biol. Rev. **62:**181–203.
29. **Howard, M., and K. Kruse.** 2005. Cellular organization by self-organization: mechanisms and models for Min protein dynamics. J. Cell Biol. **168:**533–536.
30. **Jones, L. J., R. Carballido-López, and J. Errington.** 2001. Control of cell shape in bacteria: helical, actin-like filaments in *Bacillus subtilis*. Cell **104:**913–922.
31. **Kang, C. M., D. W. Abbott, S. T. Park, C. C. Dascher, L. C. Cantley, and R. N. Husson.** 2005. The *Mycobacterium tuberculosis* serine/threonine kinases PknA and PknB: substrate identification and regulation of cell shape. Genes Dev. **19:**1692–1704.
32. **Kruse, T., J. Bork-Jensen, and K. Gerdes.** 2005. The morphogenetic MreBCD proteins of *Escherichia coli* form an essential membrane-bound complex. Mol. Microbiol. **55:**78–89.
33. **Laemmli, U. K.** 1970. Cleavage of structural proteins during the assembly of the head of bacteriophage T4. Nature **227:**680–685.
34. **Lleo, M. M., P. Canepari, and G. Satta.** 1990. Bacterial cell shape regulation: testing of additional predictions unique to the two-competing-sites model for peptidoglycan assembly and isolation of conditional rod-shaped mutants from some wild-type cocci. J. Bacteriol. **172:**3758–3771.
35. **Margolin, W.** 2006. Bacterial division: another way to box in the ring. Curr. Biol. **16:**R881–R884.
36. **Marston, A. L., and J. Errington.** 1999. Selection of the midcell division site in *Bacillus subtilis* through MinD-dependent polar localization and activation of MinC. Mol. Microbiol. **33:**84–96.
37. **Marston, A. L., H. B. Thomaides, D. H. Edwards, M. E. Sharpe, and J. Errington.** 1998. Polar localization of the MinD protein of *Bacillus subtilis* and its role in selection of the mid-cell division site. Genes Dev. **12:**3419–3430.
38. **Mazza, P., E. E. Noens, K. Schirner, N. Grantcharova, A. M. Mommaas, H. K. Koerten, G. Muth, K. Flärdh, G. P. van Wezel, and W. Wohlleben.** 2006. MreB of *Streptomyces coelicolor* is not essential for vegetative growth but is required for the integrity of aerial hyphae and spores. Mol. Microbiol. **60:**838–852.
39. **Minnikin, D. E.** 1991. Chemical principles in the organization of lipid components in the mycobacterial cell envelope. Res. Microbiol. **142:**423–427.
40. **Muchová, K., E. Kutejova, D. J. Scott, J. A. Brannigan, R. J. Lewis, A. J. Wilkinson, and I. Barak.** 2002. Oligomerization of the *Bacillus subtilis* division protein DivIVA. Microbiology **148:**807–813.
41. **Mulder, E., and C. L. Woldringh.** 1989. Actively replicating nucleoids influence positioning of division sites in *Escherichia coli* filaments forming cells lacking DNA. J. Bacteriol. **171:**4303–4314.
42. **Müller, T., R. Guggenheim, M. Düggelin, and C. Scheidegger.** 1991. Freeze-fracturing for conventional and field emission low-temperature scanning electron microscopy: the scanning cryo unit SCU 020. J. Microsci. **161:**73–83.
43. **Nyka, W.** 1974. Studies on the effect of starvation on mycobacteria. Infect. Immun. **9:**843–850.
44. **Ojha, A. K., T. K. Mukherjee, and D. Chatterji.** 2000. High intracellular level of guanosine tetraphosphate in *Mycobacterium smegmatis* changes the morphology of the bacterium. Infect. Immun. **68:**4084–4091.
45. **Panté, N., A. Jarmolowski, E. Izaurralde, U. Sauder, W. Baschong, and I. W. Mattaj.** 1997. Visualizing nuclear export of different classes of RNA by electron microscopy. RNA **3:**498–513.
46. **Ramirez-Arcos, S., M. Liao, S. Marthaler, M. Rigden, and J. A. Dillon.** 2005. *Enterococcus faecalis* divIVA: an essential gene involved in cell division, cell growth and chromosome segregation. Microbiology **151:**1381–1393.
47. **Ramos, A., M. P. Honrubia, N. Valbuena, J. Vaquera, L. M. Mateos, and J. A. Gil.** 2003. Involvement of DivIVA in the morphology of the rod-shaped actinomycete *Brevibacterium lactofermentum*. Microbiology **149:**3531–3542.
48. **Raskin, D. M., and P. A. de Boer.** 1999. Rapid pole-to-pole oscillation of a protein required for directing division to the middle of *Escherichia coli*. Proc. Natl. Acad. Sci. USA **96:**4971–4976.
49. **Rose, A., S. J. Schraegle, E. A. Stahlberg, and I. Meier.** 2005. Coiled-coil protein composition of 22 proteomes—differences and common themes in subcellular infrastructure and traffic control. BMC Evol. Biol. **5:**66.
50. **Rothfield, L., A. Taghbalout, and Y. L. Shih.** 2005. Spatial control of bacterial division-site placement. Nat. Rev. Microbiol. **3:**959–968.
51. **Sassetti, C. M., D. H. Boyd, and E. J. Rubin.** 2003. Genes required for mycobacterial growth defined by high density mutagenesis. Mol. Microbiol. **48:**77–84.
52. **Scheffers, D. J., L. J. Jones, and J. Errington.** 2004. Several distinct localization patterns for penicillin-binding proteins in *Bacillus subtilis*. Mol. Microbiol. **51:**749–764.
53. **Seiler, P., T. Ulrichs, S. Bandermann, L. Pradl, S. Jorg, V. Krenn, L. Morawietz, S. H. Kaufmann, and P. Aichele.** 2003. Cell-wall alterations as an attribute of *Mycobacterium tuberculosis* in latent infection. J. Infect. Dis. **188:**1326–1331.
54. **Shapiro, L., and R. Losick.** 1997. Protein localization and cell fate in bacteria. Science **276:**712–718.
55. **Shapiro, L., H. H. McAdams, and R. Losick.** 2002. Generating and exploiting polarity in bacteria. Science **298:**1942–1946.
56. **Shleeva, M. O., K. Bagramyan, M. V. Telkov, G. V. Mukamolova, M. Young, D. B. Kell, and A. S. Kaprelyants.** 2002. Formation and resuscitation of "non-culturable" cells of *Rhodococcus rhodochrous* and *Mycobacterium tuberculosis* in prolonged stationary phase. Microbiology **148:**1581–1591.
57. **Snapper, S. B., R. E. Melton, S. Mustafa, T. Kieser, and W. R. Jacobs, Jr.** 1990. Isolation and characterization of efficient plasmid transformation mutants of *Mycobacterium smegmatis*. Mol. Microbiol. **4:**1911–1919.
58. **Stahlberg, H., E. Kutejova, K. Muchová, M. Gregorini, A. Lustig, S. A. Muller, V. Olivieri, A. Engel, A. J. Wilkinson, and I. Barak.** 2004. Oligomeric structure of the *Bacillus subtilis* cell division protein DivIVA determined by transmission electron microscopy. Mol. Microbiol. **52:**1281–1290.
59. **Stewart, G. C.** 2005. Taking shape: control of bacterial cell wall biosynthesis. Mol. Microbiol. **57:**1177–1181.
60. **Stover, C. K., V. F. de la Cruz, T. R. Fuerst, J. E. Burlein, L. A. Benson, L. T. Bennett, G. P. Bansal, J. F. Young, M. H. Lee, G. F. Hatfull, et al.** 1991. New use of BCG for recombinant vaccines. Nature **351:**456–460.
61. **Thanky, N. R., D. B. Young, and B. D. Robertson.** 2007. Unusual features of the cell cycle in mycobacteria: polar-restricted growth and the snapping-model of cell division. Tuberculosis (Edinburgh) **87:**231–236.
62. **Thompson, J. D., D. G. Higgins, and T. J. Gibson.** 1994. CLUSTAL W: improving the sensitivity of progressive multiple sequence alignment through sequence weighting, position-specific gap penalties and weight matrix choice. Nucleic Acids Res. **22:**4673–4680.
63. **Tiyanont, K., T. Doan, M. B. Lazarus, X. Fang, D. Z. Rudner, and S. Walker.** 2006. Imaging peptidoglycan biosynthesis in *Bacillus subtilis* with fluorescent antibiotics. Proc. Natl. Acad. Sci. USA **103:**11033–11038.
64. **Triccas, J. A., T. Parish, W. J. Britton, and B. Gicquel.** 1998. An inducible expression system permitting the efficient purification of a recombinant antigen from *Mycobacterium smegmatis*. FEMS Microbiol. Lett. **167:**151–156.
65. **Walburger, A., A. Koul, G. Ferrari, L. Nguyen, C. Prescianotto-Baschong, K. Huygen, B. Klebl, C. Thompson, G. Bacher, and J. Pieters.** 2004. Protein kinase G from pathogenic mycobacteria promotes survival within macrophages. Science **304:**1800–1804.
66. **Woldringh, C. L., E. Mulder, J. A. Valkenburg, F. B. Wientjes, A. Zaritsky, and N. Nanninga.** 1990. Role of the nucleoid in the toporegulation of division. Res. Microbiol. **141:**39–49.
67. **Wolf, E., P. S. Kim, and B. Berger.** 1997. MultiCoil: a program for predicting two- and three-stranded coiled coils. Protein Sci. **6:**1179–1189.
68. **Wu, L. J., and J. Errington.** 2004. Coordination of cell division and chromosome segregation by a nucleoid occlusion protein in *Bacillus subtilis*. Cell **117:**915–925.
69. **Young, K. D.** 2003. Bacterial shape. Mol. Microbiol. **49:**571–580.